

Supporting Information for

Single-Particle Mobility Analysis Enables Ratiometric Detection of Cancer Markers under Darkfield Tracking Microscopy

Yancao Chen, Yueyue Tian, Qian Yang, Jinhui Shang, Decui Tang, Bin Xiong* and Xiao-Bing Zhang

Molecular Science and Biomedicine Laboratory, State Key Laboratory of Chemo/Biosensing and Chemometrics, College of Chemistry and Chemical Engineering, Hunan University, Changsha, 410082, P. R. China.

Email: xbs1985@hnu.edu.cn

Table of Contents

Figure S1.....	S2
Figure S2.....	S3
Figure S3.....	S4
Figure S4.....	S5
Figure S5.....	S6
Figure S6.....	S7
Figure S7.....	S8
Figure S8.....	S9
Figure S9.....	S10
Figure S10.....	S11
Figure S11.....	S12
Figure S12.....	S13
Supplementary theoretical consideration.....	S14-S15

Supplementary Figures

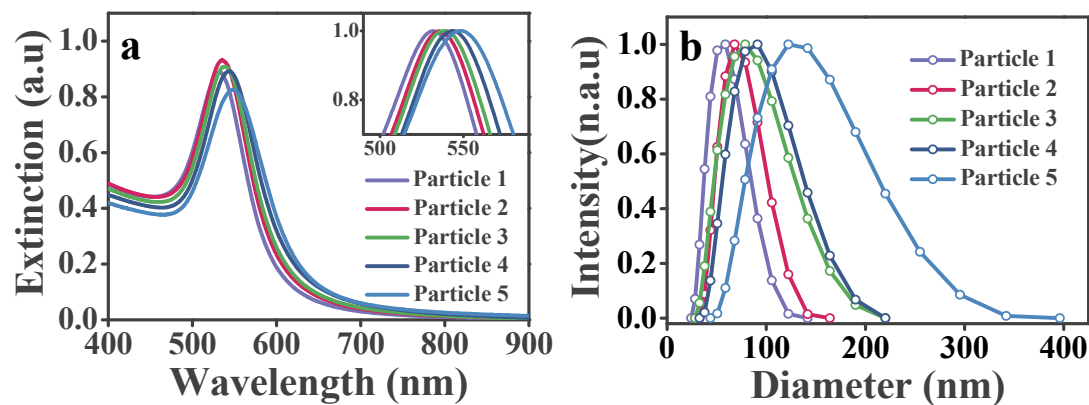


Figure S1. Characterizations of AuNPs with different diameters. UV-visible spectroscopy (a) and DLS analysis (b) for AuNPs with averaged diameters of 47.49 nm (particle 1), 59.47 nm (particle 2), 63.11 nm (particle 3), 71.20 nm (particle 4) and 79.46 nm (particle 5), respectively.

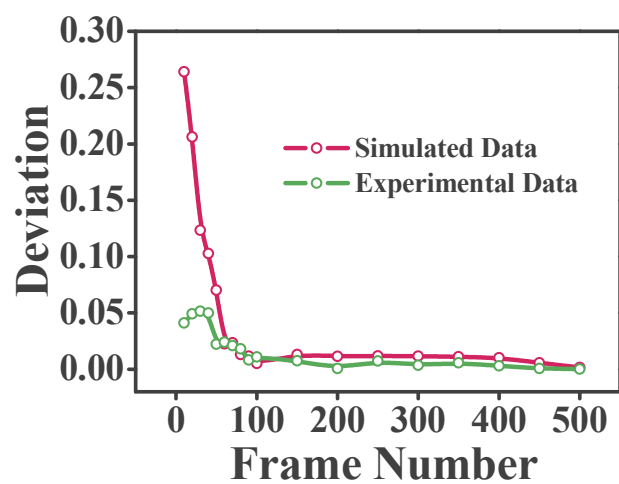


Figure S2. The deviation in hydrodynamic size as a function of frame number obtained with simulated (red dotted line) and experimental data (green dotted line), respectively.

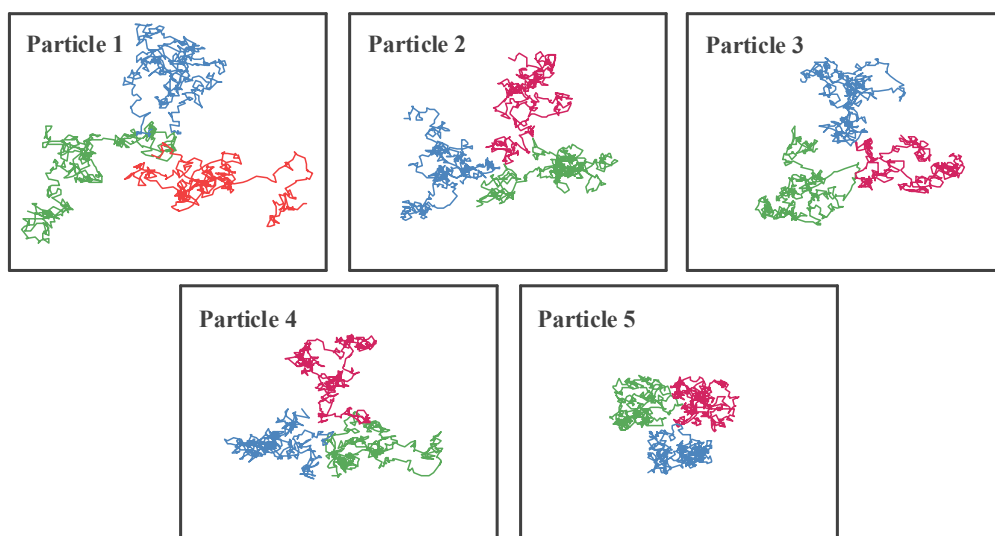


Figure S3. Representative trajectories for the five kinds of nanoparticles with averaged diameters as 47.49 nm (particle 1), 59.47 nm (particle 2), 63.11 nm (particle 3), 71.20 nm (particle 4) and 79.46 nm (particles 5), respectively.

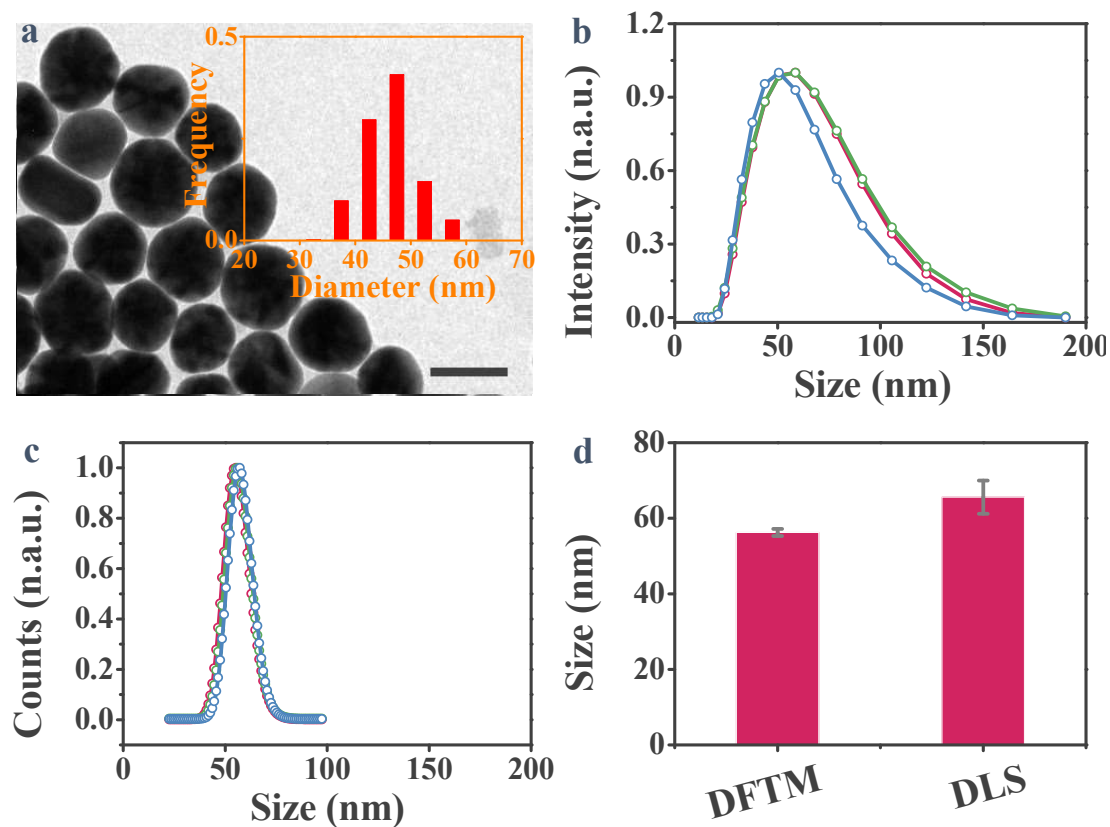


Figure S4. Characterizations of the prepared 50 nm AuNPs. (a) Representative TEM image of the AuNPs. The scale bar is 50 nm. The size distribution of AuNPs was inserted. The size distributions of AuNPs obtained by DLS analysis (b) and DFTM (c) after repeated measurements for three times. (d) The deviation in hydrodynamic size measured by DFTM and DLS analysis.

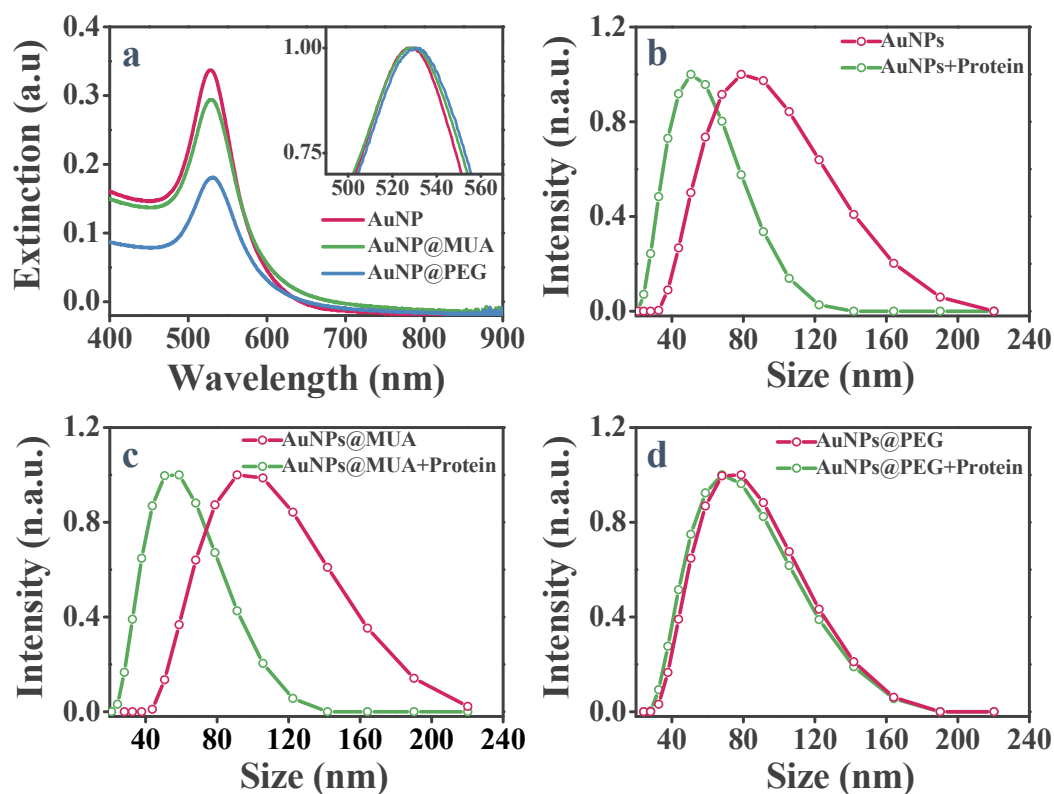


Figure S5. Characterization of AuNPs without or with surface functionalization. (a) UV-visible spectroscopy. The insert shows the peak shift for AuNPs after surface modification. DLS analysis for the hydrodynamic size of naked AuNPs (b), AuNPs@MUA (c) and AuNPs@PEG (d) before (green dotted line) and after (red dotted line) the incubation with cell culture medium.

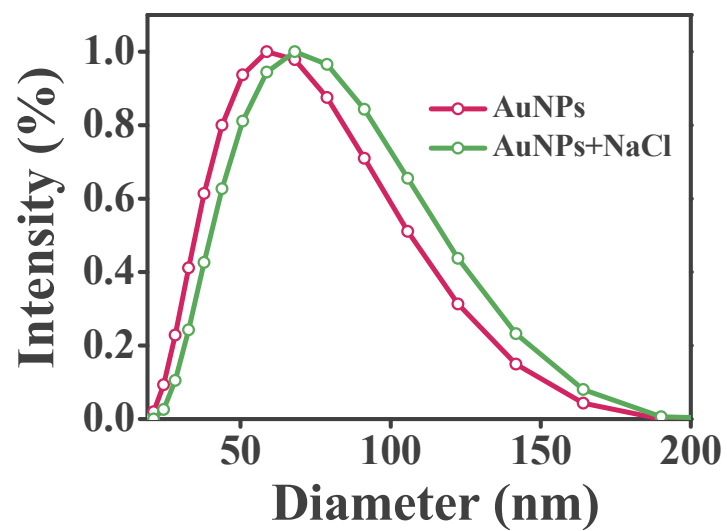


Figure S6. Size distributions of AuNPs by DLS analysis before and after NaCl treatment.

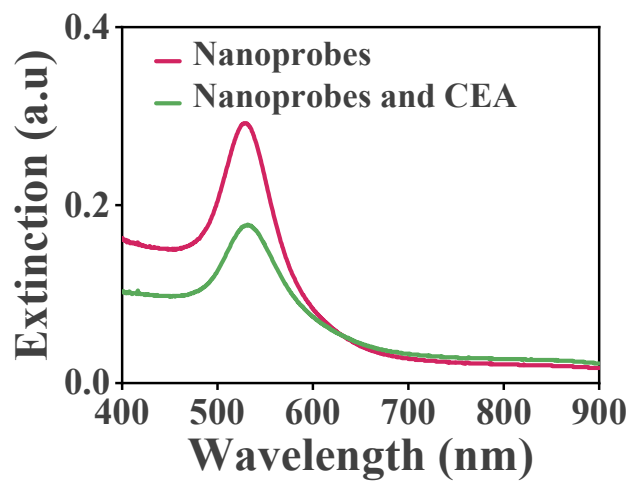


Figure S7. UV-visible spectroscopy of nanoprobes for CEA detection. Notable changes can be observed from the UV-visible spectra of nanoprobes before (red) and after (green) the addition of CEA.

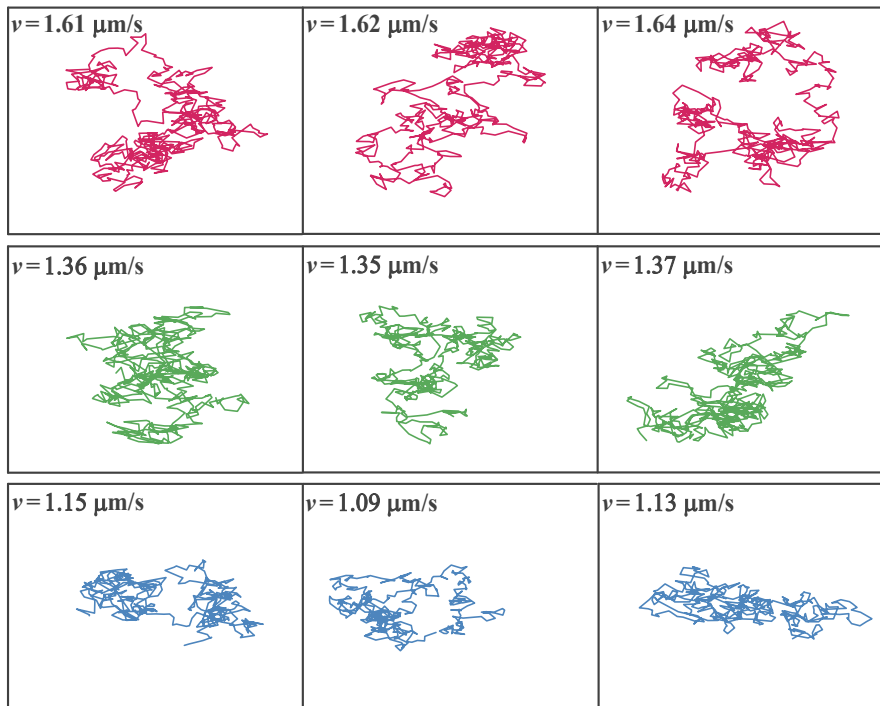


Figure S8. Representative trajectories of nanoprobe in the presence of CEA.

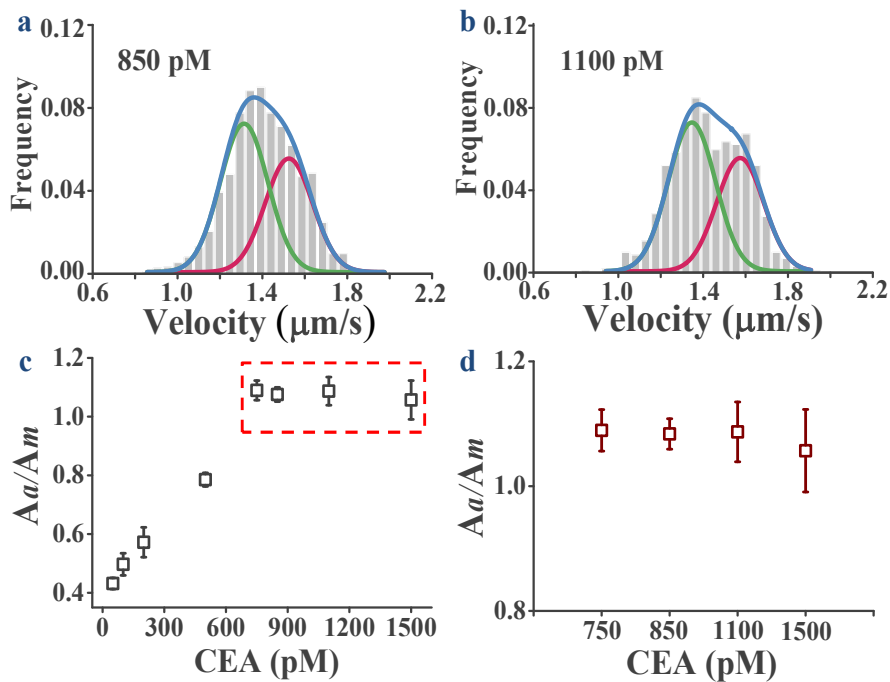


Figure S9. Investigating the influence of hook effect on sensing performance. The velocity distributions of nanoprobe in the presence of CEA at 850 pM (a) and 1100 pM (b) respectively. (c) The plots of aggregate-to-monomer ratio as a function of CEA concentration from 50 to 1500 pM. (d) The aggregate-to-monomer ratio decreased at high CEA level as labeled with the red square in (c).

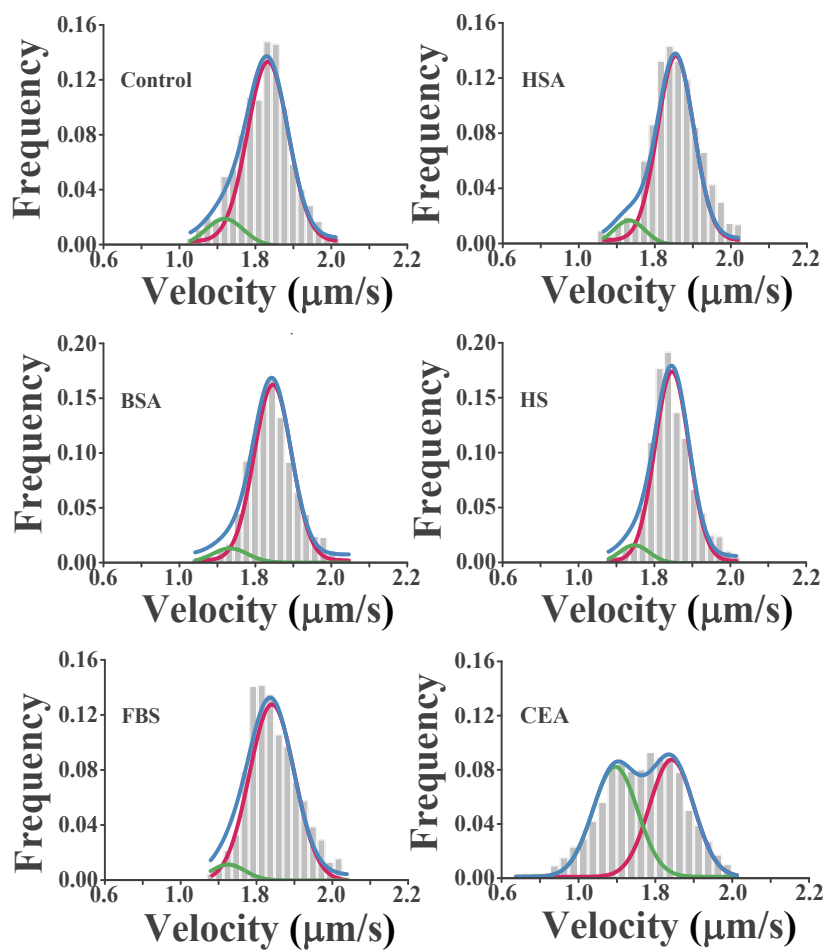


Figure S10. The velocity distributions of nanoprobe after the incubation with CEA and other proteins (or protein mixtures), respectively.

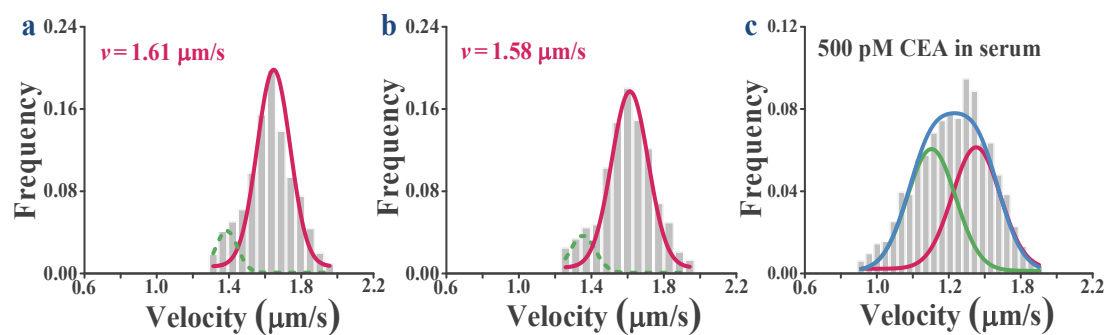


Figure S11. Testing the anti-interference ability of the ratiometric strategy. The velocity distributions of the nanoprobes before (a) and after (b) the incubation in human serum, suggesting a shift in the mean velocity of nanoprobes. (c) The velocity distributions of nanoprobes after incubated with 500 pM of CEA dispersed in serum.

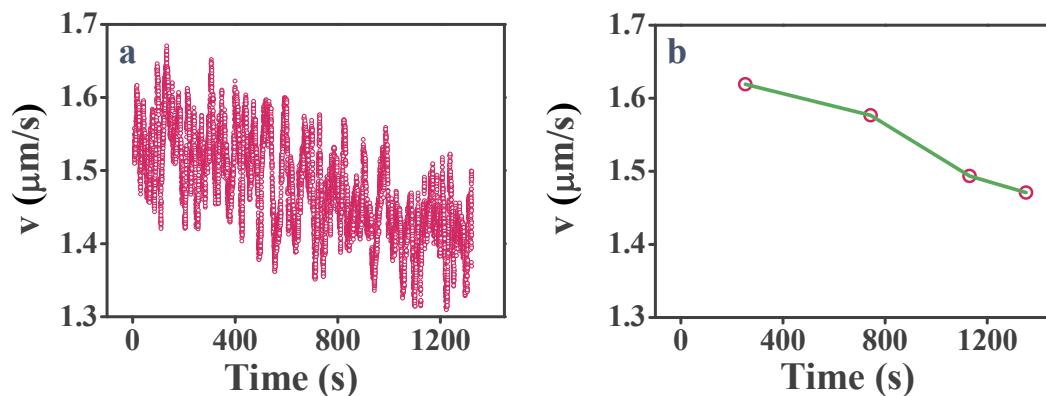


Figure S12. Investigating the seed-mediated growth of AuNPs by single-particle mobility analysis. (a) The velocity of a representative nanoparticle gradually decreased along with the increase of particle size over the growth process. (b) The averaged velocity of 237 AuNPs at different time. These results suggested the dynamics of the growth process can be analyzed from single-particle mobility analysis.

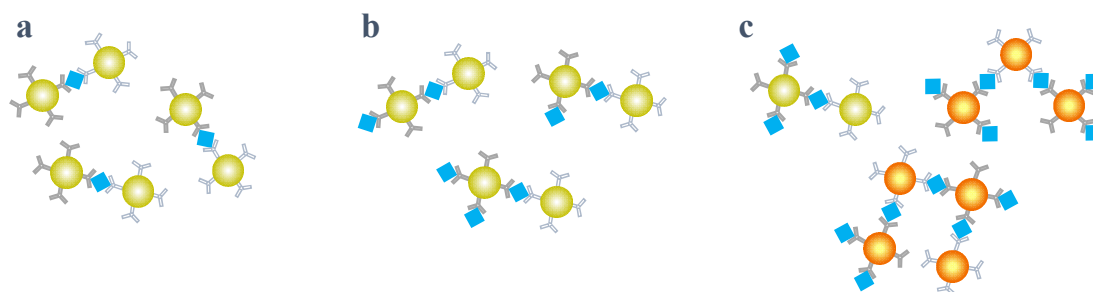
Supplementary Theoretical Consideration

Theoretical consideration for the aggregation of multivalent nanoprobe and the aggregate-to-monomer ratio as a function of CEA concentration.

For the multivalent nanoprobe, the number of antibodies conjugated on each AuNPs (Q) can be estimated from the PEG density per nm^2 (~ 1 molecule/ nm^2 , as reported in ACS Nano 2012, 6, 512-522) and the antibody concentration used for crosslinking procedure, where Q is estimated to be ~ 80 in our experiment. At low particle concentration, the aggregation of nanoprobe formed due to antigen addition was associated with the antibody-antigen interactions and the collision of nanoprobe. Therefore, the probability of aggregate formation (P) can be regarded as a function of the number of antibody on nanoprobe surface (Q), the number of antigen (N_A) as well as the initial number of nanoprobe (N_0) in the detection solution, $P = f(Q, N_A, N_0)$. Then the number of aggregate (N_a) produced due to antigen addition can be described as $N_a = N_0 \cdot f(Q, N_A, N_0)$.

At low antigen concentration, it can be anticipated that the generation of 1 aggregate consumes 2 nanoprobe (Scheme S1a), the number of monomer (N_m) can be obtained as $N_m = N_0 - 2N_a = N_0(1 - 2f(Q, N_A, N_0))$, where $N_a \leq N_0/2$. Therefore, the aggregate-to-monomer ratio (R) resulted from CEA addition can be given by $R = \frac{N_a}{N_m} = \frac{f(Q, N_A, N_0)}{1 - 2f(Q, N_A, N_0)}$. For the given nanoprobe with fixed Q and N_0 , the aggregate-to-monomer ratio (R) can be approximated as a function of antigen concentration, $R = \frac{A \cdot N_A}{1 - 2 \cdot A \cdot N_A}$, in which A is the coefficient. According to this approximation, a linear relationship between the ratio and antigen concentration might be expected at low antigen concentration ($N_A \ll 1/2A$). At moderate antigen concentration, the multivalent capture nanoprobe can bind with more than one antigen (Scheme S1b), while the number of monomer and aggregated nanoprobe would keep unchanged at the equilibrium state of association and dissociation. Then the aggregate-to-monomer ratio could approach to a maximum, given by $R \approx \max\left(\frac{A \cdot N_A}{1 - 2 \cdot A \cdot N_A}\right)$. Furthermore, more complicated aggregates can be generated in the

presence of relatively higher antigen concentration (Scheme S1c). At this situation, the aggregates formed could contain more than 2 nanoprobes. For a simplification, the number of monomer can be obtained as $N_m = N_0 - xN_a$, where x represent the averaged number of nanoprobes consumed during the formation of single aggregates. Then the aggregate-to-monomer ratio could be estimated by $R \approx \frac{A \cdot N_A}{1 - x \cdot A \cdot N_A}$, where $x > 2$. Since it is difficult to define a rigorous model for the stochastic aggregation of nanoprobes in solution, these theoretical considerations could just serve as a simplified and straightforward framework for a better understanding of targeted-induced aggregation of multivalent nanoprobes.



Scheme S1. Representative nanoprobe aggregates formed in the presence of antigen at low (a), moderate (b) and relatively higher (c) concentrations, respectively.